Journal of Applied Physics

RESEARCH ARTICLE | JANUARY 05 2024

Validation of minority carrier recombination lifetimes in low-dimensional semiconductors found by analytical photoresponses

Kai Li ; Yinchu Shen ; Zhijuan Su ; Yaping Dan

J. Appl. Phys. 135, 014301 (2024)
https://doi.org/10.1063/5.0181306

Journal of Applied Physics ARTICLE pubs.aip.org/aip/jap

Validation of minority carrier recombination lifetimes in low-dimensional semiconductors found by analytical photoresponses

Cite as: J. Appl. Phys. **135**, 014301 (2024); doi: 10.1063/5.0181306
Submitted: 16 October 2023 · Accepted: 10 December 2023 ·
Published Online: 5 January 2024

Kai Li,[1] Yinchu Shen,[1] Zhijuan Su,[2,a)] and Yaping Dan[1,a)]

AFFILIATIONS

[1]University of Michigan—Shanghai Jiao Tong University Joint Institute, Shanghai Jiao Tong University, Shanghai 200240, China
[2]Global Institute of Future Technology, Shanghai Jiao Tong University, Shanghai 200240, China

[a)]**Authors to whom correspondence should be addressed:** zhijuan.su@sjtu.edu.cn and yaping.dan@sjtu.edu.cn

ABSTRACT

It is a formidable challenge to find the minority carrier recombination lifetime in low-dimensional devices as low-dimensionality increases the surface recombination rate and often reduces the recombination lifetime to a scale of picoseconds. In this work, we demonstrated a simple but powerful method to quantitatively probe the minority carrier recombination lifetime in silicon nanowires or microwires by fitting the experimental photoresponses with our recently established analytical photoresponse principle of photoconductors. The nanowires were passivated with small molecules and Al_2O_3 to suppress surface recombination, which will increase the minority recombination lifetimes. As expected, the minority carrier recombination lifetime found by this approach increases by orders of magnitude. These wires were also made into PIN diodes, the leakage of which was reduced at least 1 order of magnitude after surface passivation by Al_2O_3. The minority recombination lifetime found from the leakage current of these devices is largely consistent with what we found from our analytical photoresponse principle. As a further step, we performed scanning photocurrent microscopy to find the minority diffusion length from which we found that the minority recombination lifetime is close to what we found from the analytical photoresponses. In short, this work validated that our analytical response principle is a reliable method to find the minority recombination lifetime in low-dimensional semiconductors.

INTRODUCTION

The down-scaling of semiconductor devices provides unlimited possibilities for emerging technologies such as flexible electronics and artificial skins in addition to the classical complementary metal–oxide–semiconductor (CMOS) technologies.[1–9] Designing these low-dimensional devices requires accurate measurements of the device parameters, which becomes increasingly difficult as the devices become small.[10–14] For example, Hall measurements are often employed to measure the doping concentration and charge carrier mobility. However, as the devices scale down, the separation between Hall electrodes becomes small, resulting in a negligibly low Hall voltage. It, thus, becomes less reliable, if not impossible, to find carrier mobility and concentration.[15–17] In recent years, we established an explicit photoresponses theory for low-dimensional photoconductors.[18] Previously, we showed that the carrier concentration and mobility in nanowire devices can be reliably found by simply fitting photoresponses with our theory.[19]

The minority carrier recombination lifetime is also an important parameter for semiconductors but quite challenging to calibrate due to the fact that the recombination lifetime becomes extremely small (often picoseconds) for nanoscale semiconductors unless an advanced apparatus is used. For example, near-field scanning photocurrent microscopy was often used to probe the minority recombination in silicon and GaAs nanowires,[20,21] which is often quite challenging since expensive near-field optical microscopy and complicated device structures (p–n junctions or Ohmic/Schottky junctions) are often required. In this work, we demonstrated that the minority carrier recombination lifetime in silicon nanowires or microwires can be readily found by fitting the experimental photoresponses with our theory. The lifetime significantly increases after the wires are passivated by grafting with small

molecules or depositing with Al_2O_3 by atomic layer deposition. We made these nanowires into PIN diodes. The leakage current of the devices is reduced by at least 1 order of magnitude after being passivated with Al_2O_3. The minority recombination lifetime can be found from the leakage current of these devices. We also performed near-field scanning photocurrent microscopy to probe the minority recombination lifetimes. The results are consistent with what we found from our analytical photoresponses theory.

RESULTS AND DISCUSSION

The silicon nanowires with five pads were made by patterning the device layer (220 nm thick) of a p-type silicon-on-insulator (SOI) wafer that was heavily doped with boron at a concentration of $\sim 10^{18}$ cm^{-3} by ion implantation with electron beam lithography followed by reactive ion etch. Photolithography and thermal evaporation were applied to form metal electrodes in contact with the five large Si pads. The overall length of the nanowires is about 27 μm with a width ranging from 50 to 900 nm. A false color scanning electron microscopic (SEM) image of a silicon nanowire device in contact with five pads is shown in Fig. 1(a). Figure 1(b) shows that the current is linear with the bias voltage for both four-probe (black) and two-probe (red) measurements, which are almost identical. Clearly, the contact between the metal electrodes and the semiconductor is Ohmic, and the contact resistances are negligible. The silicon nanowires were illuminated by a commercial LED lamp with the wavelength ranging from 520 to 525 nm. The light intensity was calibrated using a commercial diode. Figure 1(c) exhibits the conductance at a fixed bias as a function of nanowire physical width in darkness (black squares) and under light illumination (red dots). The conductance in darkness is linearly correlated with the nanowire width. This correlation, however, becomes nonlinear when the nanowire width is less than 83.4 ± 4.1 nm, which is extracted from the extension of the linear correlation [Fig. 1(c)]. The explanation of this nonlinearity is that the nanowire channel is pinched off by surface depletion regions, as shown in the schematic of Fig. 1(d). The depletion region width is ~41.7 ± 2.05 nm, half of the pinched-off nanowire width. Under light illumination, photogenerated electron–hole pairs will be physically separated by the built-in electric field in the surface depletion region, creating a forward photovoltage across the depletion regions. The forward photovoltage will consequently narrow down the depletion region width and widen the nanowire channel, consistent with our experimental observations in which the linear dependence of the nanowire current on the wire width is left-shifted to 34.9 ± 1.35 nm under light illumination.

Nanowires suffer from a high surface recombination rate due to the large surface-to-volume ratio. The surface passivation of

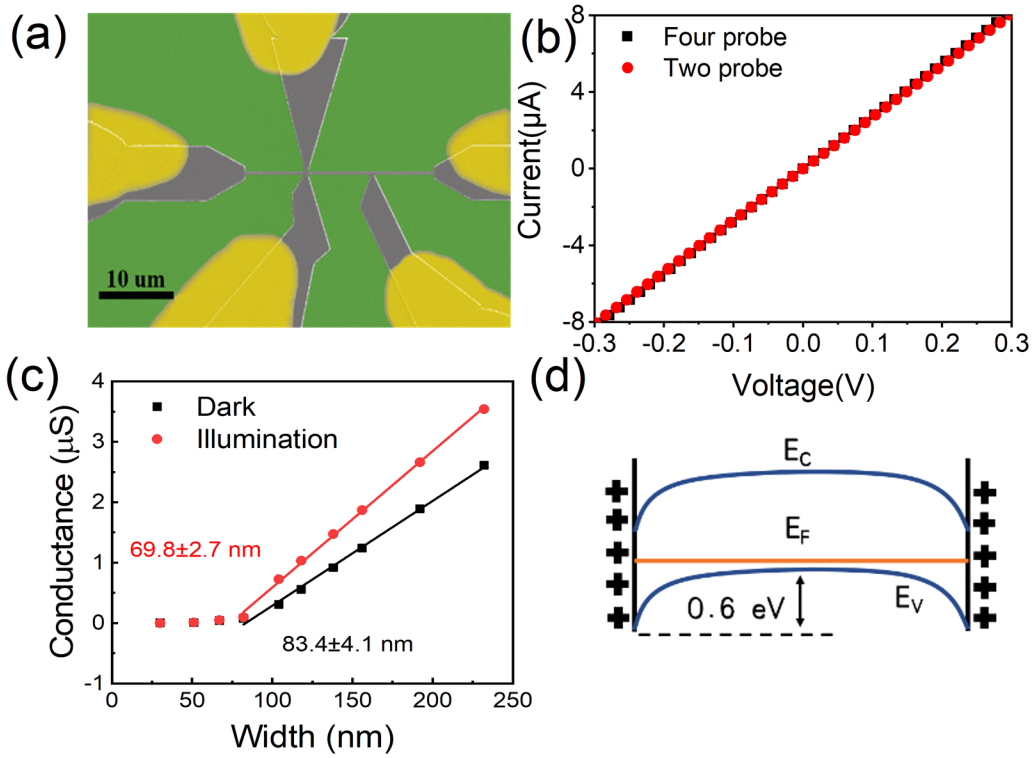

FIG. 1. (a) False color SEM image of a typical nanowire (400 nm wide); (b) I–V curves of silicon nanowires with a width of 900 nm measured by two-probe and four-probe; (c) conductance at a fixed bias of silicon nanowires with varied width in darkness and under light illumination (bias voltage is 1 V, light intensity is 2.7 mW/cm^2, wavelength λ is 520–525 nm). (d) Energy band diagram in the nanowire cross section.

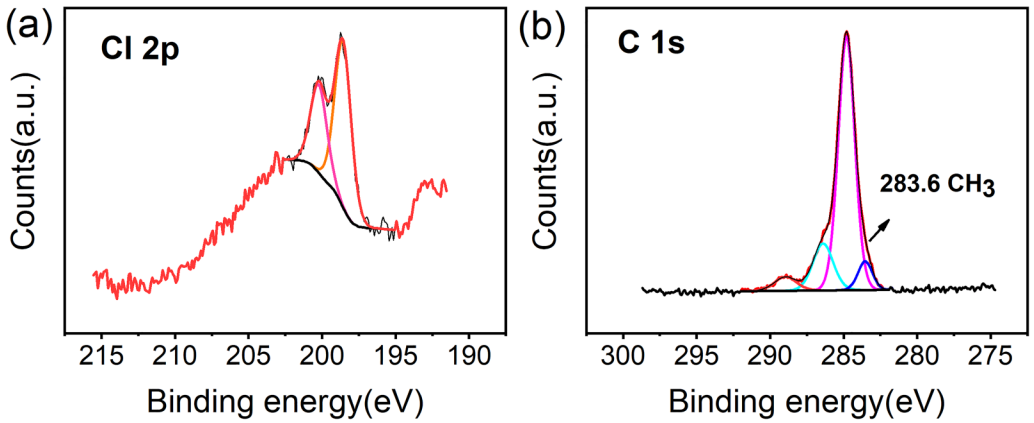

FIG. 2. XPS spectrum of (a) Si–Cl and (b) Si–CH_3.

planar optoelectronics is a technology that was developed over the course of decades. Nanowire surface passivation, however, is an even more challenging task due to their small size and the fact that multiple facets with different crystalline orientations are exposed. In this work, two methods were used to passivate the surface of silicon nanowires: one is surface chemical passivation, and the other is field effect passivation. Wet chemical surface passivation is a convenient and low-cost method, compared to other approaches that require high vacuum and high temperature. The covalent bond allows the alkyl group to graft with the silicon surface to exhibit beneficial properties, including oxidation resistance and a relatively low surface conformation rate.[22] Methyl passivation was used in this work, since it can almost completely saturate the dangling bonds on the Si (111) surface through the Si–C bond, resulting in an excellent surface order and stability. XPS characterizations were performed on the chlorine terminal sample obtained after methyl passivation. Figure 2(a) shows the binding energy information of Cl 2p of the sample. It can be seen from the figure that there are two strong peaks at 198 and 200 eV that are assigned to the Cl element. This shows that the first step of the reaction was successful to convert Si–H on the silicon surface into Si–Cl. Figure 2(b) shows the XPS spectra of C 1s after the second step reaction. A characteristic peak of Si–C appears at 283.6 eV, which shows that the second step of the alkylation reaction also successfully converted Si–Cl to Si–CH_3.

For field effect passivation, we chose Al_2O_3 as the passivation material. Al_2O_3 films are most widely used for p-type Si passivation. Due to the ultra-thin SiO_x and negatively charged interstitial O ions existing in the Al_2O_3/Si interface, the interface of the Al_2O_3 film has advantages of low interface trap density and high negative charge density. However, it also results in the fact that Al_2O_3 can only passivate p-type silicon well. In addition, the growth of Al_2O_3 by atomic layer deposition technique limits its large-scale application in the industry due to the relatively low deposition rate.[23] However, increasing the rate by high rate spatial atomic layer deposition would make the process both expensive and complex.[24] However, even so, the growth of passivated materials (Al_2O_3) by atomic layer deposition (ALD) continues to be favored by the industry. The passivation performance of the Al_2O_3/Si structure can be improved by optimizing the thickness of Al_2O_3 and annealing temperature. In this work, the ALD hydrothermal method was adopted to grow a 10 nm thick Al_2O_3 layer after a 200 nm thick Al layer was made to contact the nanowire as electrodes and activated at 425 °C for 15 min. In the two-probe and four-probe measurements, the probes can pierce the Al_2O_3 insulating layer to make direct contact with the aluminum electrode, thus achieving ohmic contact during the measurement.

The silicon nanowires were tested by the four-probe method, and the dark current vs voltage for the original wire with a width of 400 nm was obtained. As shown in Fig. 3, there is a good linear

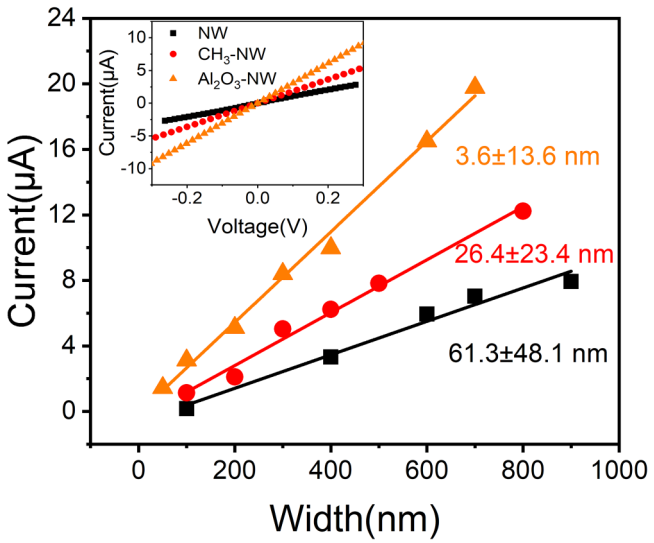

FIG. 3. Silicon nanowire current changes with nanowire width under dark field (black: unpassivated nanowires; red: nanowires passivated with methyl; yellow: nanowires passivated with Al_2O_3). Inset: I–V curves of Si wires (400 nm).

TABLE I. Results of extraction and calculation of nanowires after fitting by Eq. (1).

Sample	Width (nm)	$\frac{\eta kT}{2qV_{bi0}} I^s_{ph}$ (nA)	P^s_{light} (μW/cm^2)	α	τ_0 (ns)	V_{srv} (10^2 cm/s)
NWs	900	97.64 ± 12.38	583.44 ± 136.53	0.29	0.35 ± 0.07	245.31 ± 57.42
	700	35.04 ± 1.51	313.67 ± 29.11	0.25	0.74 ± 0.06	109.16 ± 10.13
	400	35.63 ± 2.55	371.77 ± 54.87	0.76	0.21 ± 0.03	332.14 ± 49.07
CH_3–NWs	900	16.23 ± 0.39	16.76 ± 1.48	0.29	12.08 ± 0.98	7.05 ± 0.62
	700	7.08 ± 0.10	10.30 ± 0.55	0.25	22.53 ± 1.14	3.58 ± 0.19
	400	6.36 ± 0.47	35.73 ± 8.86	0.76	2.16 ± 0.43	31.92 ± 7.92
Al_2O_3–NWs	900	1.76 ± 0.03	9.31 ± 0.53	0.29	21.73 ± 1.17	3.91 ± 0.22
	700	1.17 ± 0.02	6.60 ± 0.44	0.25	35.20 ± 2.20	2.30 ± 0.15
	400	0.79 ± 0.02	4.47 ± 0.52	0.76	17.23 ± 1.80	3.99 ± 0.47

relationship between the dark current and voltage. The I–V curves of the nanowires passivated with methyl and Al_2O_3 are also shown. The linearity between the dark current and voltage is not affected by the passivation process. The current under a fixed bias for wires with and without passivation is shown in Fig. 3. It is seen that the dark current is directly proportional to the width of the nanowire. The intersection of the fitting line with x axis is twice the width of the depletion region, which is caused by surface states and fixed charges. The width of the depletion region of the unpassivated nanowires is ∼30.65 ± 24.05 nm, which was reduced to ∼13.2 ± 12.7 and ∼1.8 ± 6.8 nm after the nanowires were passivated with methyl and Al_2O_3, respectively, as shown in Fig. 3. Note that for these well-passivated nanowires, there is a relatively large uncertainty in the actual depletion region width. As a result, the extracted minority recombination lifetimes found in Table I also have a relatively large uncertainty. Ideally, a set of narrower nanowires should be fabricated, which is subject to future work.

Under light illumination, which was switched ON and OFF periodically, the wire current increases and decreases accordingly [inset in Fig. 4(a)]. The photocurrent dependent on the light intensity is plotted in Figs. 4(a)–4(c) for the unpassivated, methyl passivated, and Al_2O_3 passivated nanowires, respectively. This

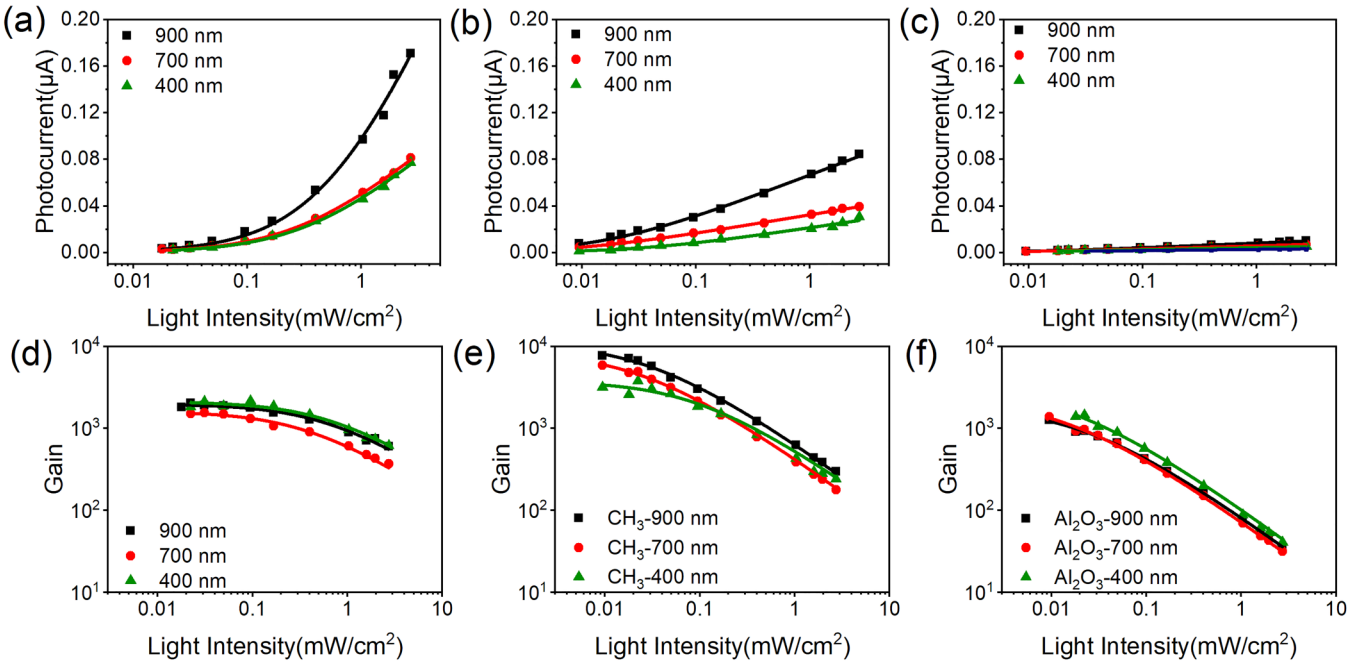

FIG. 4. Photocurrent of silicon wires dependent on the light intensity and corresponding fitting curves: (a) NWs; (b) CH_3–NWs; (c) Al_2O_3–NWs; photogain of silicon wires: (d) NWs, (e) CH_3–NWs, and (f) Al_2O_3–NWs.

dependency is governed by the following equation as shown in our previous work:[18]

$$I_{ph} = \frac{\eta kT}{2qV_{bi0}} I^s_{ph} ln\left(\frac{P_{light}}{P^s_{light}} + 1\right), \quad (1)$$

where $I^s_{ph} = \mu_p pqE_{ch} W_{dep} \left|\frac{dA_{ch}}{dW_{dep}}\right|$ is defined as the photocurrent when the depletion region shrinks to zero by light illumination; $P^s_{light} = \frac{\hbar\omega J_s H}{\alpha W_{dep} q}$ is defined as the critical light intensity, which creates a photocurrent density across the junction equal to the junction leakage current density; J_s is the leakage current density of the Schottky junction as $J_s = \frac{qn_i W_{dep}}{2\tau_0}$ with q being the unit charge, n_i being the electron concentration in intrinsic silicon, and W_{dep} being the depletion region width; V_{bio} is the surface potential in the dark; η is the ideality factor; kT is the thermal energy; E_{ch} is the electric field intensity in the nanowire; W_{dep} is the width of the depletion region; dA_{ch} is the change in the cross-sectional area of the nanowire channel; dW_{dep} is the change in the width of the depletion region; H is the physical height of the nanowire; and α is the light absorption ratio.

Equation (1) can well fit the experimental data in Figs. 4(a)–4(c). From the fittings, we extract $\frac{\eta kT}{2qV_{bi0}} I^s_{ph}$ and P^s_{light} in Table I. From P^s_{light}, we can further find J_s after the light absorption coefficient α is calculated by the finite difference time domain (FDTD) method. The effective minority recombination lifetime τ_0 can be found from the correlation with J_s as $J_s = \frac{qn_i W_{dep}}{2\tau_0}$, which is in the sub-nanosecond range for unpassivated nanowires (see Table I) but increases to tens of nanoseconds, largely consistent with literature reports.[20] For low-dimensional devices, the effective minority carrier recombination lifetime τ_0 is closely related to the surface recombination rate, which is given in the following equation in the case of nanowires with rectangular cross section:[19]

$$\frac{1}{\tau_0} = \frac{1}{\tau_b} + \frac{2V_{srv}}{W} + \frac{2V_{srv}}{H}, \quad (2)$$

in which τ_b is the minority recombination lifetime in the bulk semiconductor, which is at a scale of microseconds at a doping concentration of 10^{18} cm^{-3}, W is the nanowire width, and H is the nanowire thickness. The surface recombination velocity of the etched nanowires is on the same order of magnitude with the chemically synthesized ones. Al_2O_3, indeed, offers the best passivation effect by reducing the surface recombination velocity by 2 orders of magnitude. Note that the 700 nm-wide nanowire has a consistently higher minority recombination lifetime than the 900 nm-wide nanowire, which is probably because the 700 nm-wide nanowire happens to have a higher surface quality.

Photogain dependence on the light intensity can be further obtained from Eq. (1) according to the definition of external quantum efficiency,

$$G = \frac{I_{ph}/q}{I_{light} A_{proj}/\hbar\omega} = G_{\max} \frac{P^s_{light}}{P_{light}} \ln\left(\frac{P_{light}}{P^s_{light}} + 1\right), \quad (3)$$

where $G_{\max}$ is shown in the following equation:

$$G_{\max} = \frac{n_1 \hbar\omega kT I^s_{ph}}{2q^2 V_{bi0} A_{proj} I^s_{light}} = \frac{2\alpha\varepsilon_s nkT \left|\frac{dA_{ch}}{dW_{dep}}\right|}{q^2 n_i W_{dep} A_c} \frac{\tau_0}{\tau_t}, \quad (4)$$

where A_c is the cross-sectional area of nanowires; and τ_t is the transit time of the majority carrier across the photoconductor, $\tau_t = \frac{L}{\mu_p E_{ch}}$, where L is the nanowire length, μ_p is the majority carrier mobility, and E_{ch} is the electric field intensity along the channel.

The photogain is proportional to the photocurrent divided by the light intensity. It reaches its maximum as the light intensity approaches zero. A nearly zero light intensity is difficult to accurately calibrate. As a result, the dominant large photogain has a relatively large uncertainty. For this reason, we extracted the device physical parameters by fitting the photocurrent equation (1) to the experimental data in Figs. 4(a)–4(c). In the past, it was often believed that high photogain of low-dimensional photoconductors comes from the trapping effect of surface states. A higher density of surface states will lead to more photosensitive photoconductors. A first sight of Figs. 4(a)–4(c) seems consistent with this conclusion; i.e., the nanowire is more photosensitive if poorly passivated. However, a closer look at the photogain in Figs. 4(d)–4(f) shows a more complicated picture. This is because the photoresponse is determined by the interplay of the surface depletion region width and surface recombination velocity. For unpassivated devices, a high concentration of surface states results in a wider surface depletion region and a larger surface recombination velocity. Accordingly, $\frac{\eta kT}{2qV_{bi0}} I^s_{ph}$ and P^s_{light} in Eq. (1) are both larger as well, which, however, has a competing effect in the photocurrent. As a result, the moderately passivated nanowires by methyl are more photosensitive at low light intensity [Fig. 4(e)]. A strategy to decouple the completing effect of the surface depletion region and surface recombination velocity is to use core–shell nanowires, such as core–shell PN junction nanowires[25] or heterojunction nanowires,[20] in which the depletion region and interface are away from the surfaces.

To validate our conclusion drawn from the fittings above, we fabricated a set of PIN junction silicon wires with the width from 200 to 900 nm to compare their leakage current before and after Al_2O_3 passivation. It is well known that the leakage current density J_s of a reversely biased PIN junction is inversely proportional to its effective minority recombination lifetime in the depletion region following the aforementioned equation $J_s = \frac{qn_i W_{dep}}{2\tau_0}$. After passivation, the effective minority recombination lifetime will increase by orders of magnitude, resulting in a significant drop in the leakage current. Our silicon wires are 5 μm long with two large silicon pads, fabricated by patterning a lightly doped SOI wafer. The large silicon pads were highly doped with boron and phosphorus both at 1×10^{18} cm^{-3}, as shown in the false color SEM image in the inset in Fig. 5(a). The I–V curves of PIN diodes with an applied voltage range between ±10 V were measured. Figure 5(a) shows the current vs voltage (I–V) of PIN diodes without passivation. The leakage current of the PIN diodes without passivation is around

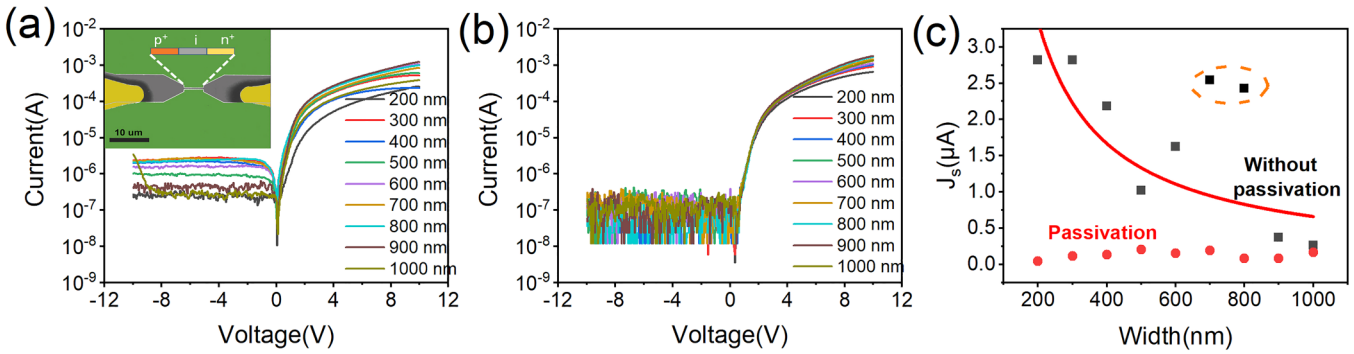

FIG. 5. I–V curves of PIN structure nanowires (a) without an Al_2O_3 layer and (b) with an Al_2O_3 layer; (c) the relationship between the leakage current and the width of the nanowire. Inset in panel (a) is the schematic structure of the p–i–n nanowire.

2.7×10^{-7}–2.3×10^{-6} A at a reverse bias of −10 V. The reverse leakage current of the PIN diodes with the Al_2O_3 passivation layer is about 1.2×10^{-8}–2.4×10^{-7} A. Statistically, the leakage current after surface passivation is reduced by at least 1 order of magnitude, consistent with the fact that surface passivation is, indeed, effective in reducing surface recombination,

$$J_s = \frac{qn_i W_{dep}}{2}\left(\frac{1}{\tau_b} + \frac{2V_{srv}}{W} + \frac{2V_{srv}}{H}\right). \quad (5)$$

We derived a new equation as Eq. (5) by combining the expressions for J_s and τ_0 shown above, which describes the relationship between the leakage current and the width of the nanowire. The leakage current is inversely proportional to the width. With the exception of the 700 and 800 nm-wide nanowires (in orange dashed circle), Eq. (5) fits well with the experimental data in Fig. 5(c). After surface passivation, the surface recombination velocity V_{srv} drops by 1–2 orders of magnitude, as a result of which the leakage current density J_s becomes nearly independent of the nanowire width. This observation is consistent with the parameters extracted in Table I.

We have to admit that the above work indirectly validates the minority carrier lifetime found by our analytical photoresponses. To directly measure the minority carrier recombination lifetime, we employed near-field scanning photocurrent microscopy.[20] This method utilizes a near-field scanning optical microscope to scan the nanowires. The presence of a nanoscale illumination point at the probe tip enables the generation of excess carriers outside the depletion region (i-region), which undergo rapid recombination and diffuse in the absence of an electric field. The depletion region collects a portion of these carriers that arrive at the border by diffusion. The topography (i.e., AFM image) and photocurrent map were simultaneously obtained, as shown in Fig. 6(a). The photocurrent decays exponentially as the illumination spot moves away from the depletion region border along the nanowire axis [Fig. 6(b)].

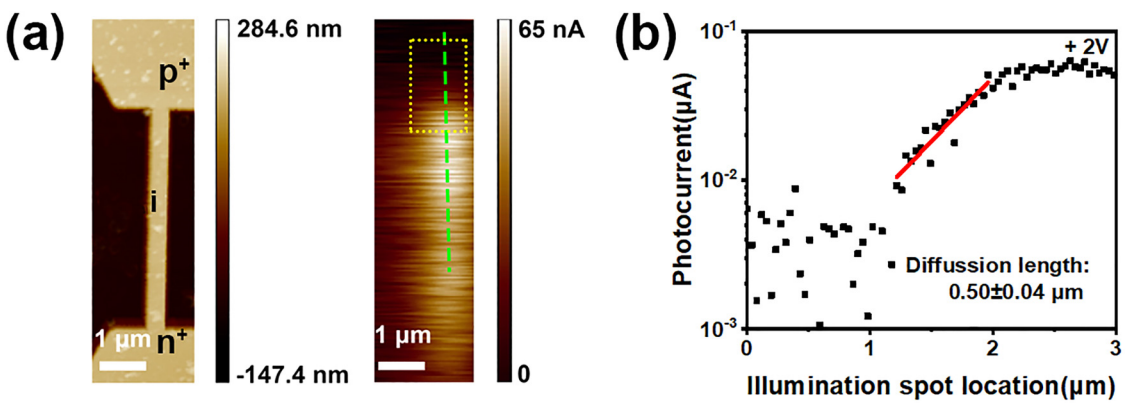

FIG. 6. (a) Topography (left) of the nanowire with a width of 200 nm obtained through atomic force microscopy; photocurrent map (right), recorded simultaneously with the topographic image; (b) photocurrent profile along the nanowire axis [green dashed line of panel (a) and data were collected in the yellow dashed area near the p–i boundary], and the applied voltage is 2 V.

The diffusion length (L_{diff}) can be extracted from the exponential relationship between the photocurrent and the position of the illumination point. In the end, the minority carrier lifetime (τ) can be calculated using the following equation:

$$L_{diff} = (D\tau)^{1/2}, \quad (6)$$

where $D = 4.0\ cm^2/s$ with mobility $\mu = 155 \pm 10\ cm^2/(V\ s)$.[18]

From Fig. 6(b), we find a diffusion length of 504.8 ± 41.6 nm and a minority carrier lifetime of 0.64 ± 0.10 ns for a PIN junction with a width of 200 nm. These values are consistent with the minority carrier lifetime previously obtained for the unpassivated nanowire shown in Table I.

Clearly, the experimental observation on the PIN diodes further validates our analytical photoresponse principle for photoconductors in addition to the Hall measurement results in our previous publication.[19]

CONCLUSIONS

In this work, we have successfully increased the effective minority recombination lifetime of nanowires nearly 2 orders of magnitude by surface passivation with a 10 nm thick Al_2O_3 layer. The effective minority recombination lifetime is extracted from our previously established explicit photogain principle by fitting to experimental photoresponses of nanowire photoconductors. PIN junction silicon wires show a significant drop in the leakage current after Al_2O_3 passivation. Statistically, the leakage current after surface passivation is reduced by at least 1 order of magnitude due to the effective passivation of Al_2O_3, largely consistent with the parameters extracted from our analytical photoresponse principle. It is, therefore, reliable to use our analytical photoresponse principle for photoconductors to extract the parameters of low-dimensional devices that are often challenging to find.

EXPERIMENTAL METHODS

Si nanowire fabrication

The silicon-on-insulator (SOI) wafers with a 220 nm thick top silicon layer were first cleaned with acetone, ethanol, and de-ionized water. Boron ions were then implanted into the device layer of the SOI wafer at an implantation energy of 30 keV and a dose of $2.2 \times 10^{13}\ cm^{-2}$. The peak doping is located at 110 nm with a maximum doping concentration of $\sim 1 \times 10^{18}\ cm^{-3}$. A rapid thermal annealing (RTA) is performed at 1000 °C for 20 s to activate the implanted boron atoms. Afterward, the activated SOI wafers were cut into squares ($\sim 1 \times 1\ cm^2$). The cut pieces were cleaned with piranha solution at 120 °C for 60 min to remove organic contaminations.

The polymethyl methacrylate (PMMA) resist (XR-1541-006, Dow Corning Electronics, USA) was spin-coated on the p-type SOI samples at 4000 rpm for 60 s to form a 250 nm thick anti-reagent layer and then bake at 180 °C for 90 s. The PMMA resist was exposed by electron beam lithography (Vistec EPBG5200) and subsequently developed in MIBK and IPA. Then, a 70 nm thick aluminum (Al) metal layer was evaporated on the silicon wafer, followed by a liftoff process in acetone. In this way, the metal mask layer of the nanowire was formed. To form an etch mask for the electrodes, NR9-1500PY (Futurrex Inc., USA) photoresist was coated on the wafers at 4000 rpm for 40 s. After baking at 140 °C for 60 s, the NR9 resist was exposed to UV light (MDA-400) and developed in the developer after post-baking at 100 °C for 60 s. A 200 nm thick Al film was evaporated (Thermal Evaporator, Angstrom Engineering), followed by a liftoff process. The Al nanowire and electrode patterns defined by electron beam exposure and photolithography were then transferred to the SOI device layer by reactive ion etching (RIE, Sentech ICP Reactive Ion Etching System). Photolithography and the thermal evaporation process were performed in the same way again, with another 200 nm thick Al metal layer grown on the electrode part, and then annealed in an argon atmosphere at 230 °C for 20 min to make a good ohmic contact between metal and silicon.

Passivation of nanowires with methyl

(1) Surface cleaning of nanowires: The nanowires were washed sequentially with acetone, ethanol, and de-ionized water and then soaked in Piranha solution [98% H_2SO_4:30% H_2O_2, 3:1 (v/v)], and heated at 120 °C for 30 min to remove the aluminum electrode on the surface. After heating, the nanowires were slowly cooled to room temperature, and then diluted and washed with de-ionized water. (2) Hydrogen termination of Si samples: The cleaned nanowires were soaked in HF aqueous solution (2.5 wt. %) for 30 s, taken out and rinsed with de-ionized water, and then immediately immersed in NH_4F aqueous solution for 18 s. (3) Chlorination of H–Si: The H–Si samples were placed into a saturated chlorobenzene solution with PCl_5 for chlorination, with a small amount of benzoyl peroxide particles (free radical initiator) adding to the reaction solution. The entire reaction was heated at 100 °C for 60 min. After the reaction, the nanowires were cooled to room temperature, removed from the reaction solution, and washed with chlorobenzene solvent and tetrahydrofuran (THF) solvent in sequence. (4) Alkylation of Cl–Si samples: The chlorinated samples were put into 1.0 M methyl magnesium chloride solution (it can be obtained by diluting 3 M CH_3MgCl solution with THF). The reaction continued at 65 °C for 2–3 h. After the reaction, the nanowires were taken out and washed in THF, methanol, and de-ionized water in sequence.

Passivation of nanowires with Al2O3

Before the growth of Al_2O_3, surfaces of the electrode need to be cleaned with Piranha solution [98% H_2SO_4:30% H_2O_2, 3:1 (v/v)]. Then, 2.5% HF was used to remove surface oxides, and finally, the nanowires were immersed in the concentrated nitric acid solution and heated at 125 °C for 15 min. This treatment was to form a 1–2 nm SiO_2 layer on the silicon surface. The presence of a thin layer of SiO_2 would facilitate passivation with Al_2O_3. In the process of Al_2O_3 growth by ALD, the precursor pulse time was 0.4 s and then rinsed with Ar for 3 s, the total reactant pulse time was 0.3 s, the rinse time was 3 s, the rinse gas flow was 600 SCCM, the substrate temperature was 300 °C, and the growth rate of Al_2O_3 was 0.1 nm/s. After growth, the samples were annealed at a temperature of 425 °C for 15 min in a nitrogen atmosphere to activate alumina.

Fabrication of PIN junctions

The same SOI silicon wafers were used to fabricate PIN junctions. In addition, the same process was used to make PIN structures. Boron ions with a concentration $\sim 1 \times 10^{18}\,\mathrm{cm}^{-3}$ were implanted into one of the electrodes of PIN, while the other electrode was implanted with phosphorous ions with a concentration $\sim 1 \times 10^{18}\,\mathrm{cm}^{-3}$. Finally, the aluminum electrodes were evaporated on the corresponding areas.

Optoelectronic measurement

The devices were characterized in a probe station by high-precision digital sourcemeters (Keithley 6487 and 2636). Light from a commercial LED ($\lambda = 520$–525 nm) forms a uniform light illumination spot (~5 mm in diameter) on the samples. The light intensity is controlled by the driving current of the circuit. The light intensity is calibrated by a commercial photodiode (G10899-003K, Hamamatsu).

Near-field scanning optical microscope measurement

A near-field optical scanning microscope (NTEGRA Solaris Probe NanoLaboratory) was externally connected to the probe, a lock-in amplifier (Model SR830 DSP), and a high-precision digital sourcemeters (Keithley 2400), which were used to scan the photocurrent and surface morphology simultaneously. The scanning speed was 0.05 HZ.

ACKNOWLEDGMENTS

This work was financially supported by the special-key project of Innovation Program of Shanghai Municipal Education Commission (No. 2019-07-00-02-E00075), the National Science Foundation of China (NSFC) (No. 92065103), the Oceanic Interdisciplinary Program of Shanghai Jiao Tong University (No. SL2022ZD107), the Shanghai Jiao Tong University Scientific and Technological Innovation Funds (No. 2020QY05), and the Shanghai Pujiang Program (No. 22PJ1408200). The devices were fabricated at the Center for Advanced Electronic Materials and Devices (AEMD), and XPS measurements were carried out at the Instrumental Analytical Center (IAC), Shanghai Jiao Tong University.

AUTHOR DECLARATIONS

Conflict of Interest

The authors have no conflicts to disclose.

Author Contributions

Kai Li: Data curation (lead); Investigation (lead); Methodology (lead); Visualization (lead); Writing – original draft (lead). **Yinchu Shen:** Data curation (supporting); Formal analysis (supporting); Investigation (supporting). **Zhijuan Su:** Conceptualization (equal); Funding acquisition (equal); Project administration (equal); Supervision (equal); Writing – review & editing (equal). **Yaping Dan:** Conceptualization (equal); Formal analysis (equal); Funding acquisition (equal); Methodology (equal); Project administration (equal); Resources (equal); Supervision (equal); Validation (equal); Writing – review & editing (equal).

DATA AVAILABILITY

The data that support the findings of this study are available from the corresponding authors upon reasonable request.

REFERENCES

[1]S. Huang, Y. Liu, Y. Zhao, Z. Ren, and C. F. Guo, Adv. Funct. Mater. **29**, 1805924 (2019).
[2]K. Keum, J. W. Kim, S. Y. Hong, J. G. Son, S.-S. Lee, and J. S. Ha, Adv. Mater. **32**, 2002180 (2020).
[3]Y. Khan, A. Thielens, S. Muin, J. Ting, C. Baumbauer, and A. C. Arias, Adv. Mater. **32**, 1905279 (2020).
[4]H.-R. Lim, H. S. Kim, R. Qazi, Y.-T. Kwon, J.-W. Jeong, and W.-H. Yeo, Adv. Mater. **32**, 1901924 (2020).
[5]K. Liu, B. Ouyang, X. Guo, Y. Guo, and Y. Liu, npj Flexible Electron. **6**, 1 (2022).
[6]P. Wang, M. Hu, H. Wang, Z. Chen, Y. Feng, J. Wang, W. Ling, and Y. Huang, Adv. Sci. **7**, 2001116 (2020).
[7]J. J. Kim, Y. Wang, H. Wang, S. Lee, T. Yokota, and T. Someya, Adv. Funct. Mater. **31**, 2009602 (2021).
[8]K. Xu, Y. Lu, and K. Takei, Adv. Mater. Technol. **4**, 1800628 (2019).
[9]C. Zhao, Y. Wang, G. Tang, J. Ru, Z. Zhu, B. Li, C. F. Guo, L. Li, and D. Zhu, Adv. Funct. Mater. **32**, 2110417 (2022).
[10]X. Gao, B. Guan, A. Mesli, K. Chen, and Y. Dan, Nat. Commun. **9**, 118 (2018).
[11]D. V. Lang, J. Appl. Phys. **45**, 3023 (1974).
[12]W. Gotz, G. Pensl, and W. Zulehner, Phys. Rev. B **46**, 4312 (1992).
[13]A. L. Endros, W. Kruhler, and F. Koch, J. Appl. Phys. **72**, 2264 (1992).
[14]M. T. Asom, J. L. Benton, R. Sauer, and L. C. Kimerling, Appl. Phys. Lett. **51**, 256 (1987).
[15]L. Barbut, F. Jazaeri, D. Bouvet, and J.-M. Sallese, IEEE Trans. Electron Devices **61**, 2486 (2014).
[16]J. Pascal, L. Hebrard, V. Frick, J.-B. Kammerer, and J.-P. Blonde, Sens. Actuators A **152**, 21 (2009).
[17]Y. Shimazu, T. Iwabuchi, K. Arai, and I. Shioya, Phys. Lett. A **384**, 126073 (2020).
[18]J. He, K. Chen, C. Huang, X. Wang, Y. He, and Y. Dan, ACS Nano **14**, 3405 (2020).
[19]K. Li, J. He, W. Zhang, H. Liu, and Y. Dan, IEEE Electron Device Lett. **43**, 422 (2022).
[20]Y. P. Dan, K. Seo, K. Takei, J. H. Meza, A. Javey, and K. B. Crozier, Nano Lett. **11**, 2527 (2011).
[21]C. Gutsche, R. Niepelt, M. Gnauck, A. Lysov, W. Prost, C. Ronning, and F. J. Tegude, Nano Lett. **12**, 1453 (2012).
[22]X. Zhao, P. Tu, J. He, H. Zhu, and Y. Dan, Nanoscale **10**, 82 (2018).
[23]J. A. García-Valenzuela, R. Rivera, A. B. Morales-Vilches, L. G. Gerling, A. Caballero, J. M. Asensi, C. Voz, J. Bertomeu, and J. Andreu, Thin Solid Films **619**, 288 (2016).
[24]F. Werner, W. Stals, R. Görtzen, B. Veith, R. Brendel, and J. Schmidt, Energy Procedia **8**, 301 (2011).
[25]J. J. He, C. L. Huang, H. M. Wen, X. M. Wang, Y. N. He, and Y. P. Dan, Nanotechnology **31**, 195201 (2020).